



An updated analytical method for predicting the bracing behavior of Z-purlin supported standing seam diaphragm systems

Michael W. Seek¹

Abstract

Roof systems utilizing Z-purlins as a secondary member supporting a standing seam panel system are used extensively by the metal building industry. The Z-purlins rely on the diaphragm action in the standing seam panel system to provide lateral support and transfer forces to anchorages. The behavior of the standing seam system is highly nonlinear making prediction of the interaction between the Z-purlin and the standing seam system difficult. To better understand the behavior of the interaction between the purlins and the panel system, a series of non-linear shell finite element models were developed based on the test results of simple span systems. These models capture the non-linear flexibility of the connection between the purlin and the panel and show good correlation to the tests. Based on the results of the finite element models, an analytical method to predict the forces interacting between the purlin and the sheathing as well as the resulting diaphragm deformation was developed. This analytical method provides a foundation for additional analytical methodologies to predict the strength and stability of Z-purlin and standing seam panel systems

1. Introduction

Cold formed steel purlins in roof systems rely on the panels attached to the top flange to provide lateral restraint through diaphragm action. There are two main types of panel systems: through-fastened and standing seam. Through-fastened panels are directly fastened to the top flange of the purlin with a self-tapping screw whereas standing seam panel systems have a clip that connects the purlin to the panels. The clip has a tab that fits into the seam of the panels and the clip is fastened to the purlin with self-tapping screws. Clips may either be fixed or sliding. For sliding clips, the tab connected to the seam can move relative to the base of clip connected to the purlin to accommodate thermal movements in the panels. Because of the clip connection, standing seam panel systems typically have a much lower diaphragm stiffness than through-fastened systems. Some of the reduced stiffness results from slip in the seams between the panels and some results from slip in sliding clips or deformation of fixed clips.

Because the purlins rely on the diaphragm action in the panels for stability, AISI S100 (AISI, 2016) requires that a continuous path for the restraining forces be analyzed to transfer the forces through the panel system to the anchorage devices. Original methods to evaluate this transfer of

¹ Associate Professor, Old Dominion University, <mseek@odu.edu>

forces through the panels to the anchorage devices were based on the through-fastened systems (Seek and Murray, 2008) and utilized pure shear behavior in the panels. The effective shear stiffness, G' , of the purlin and panel system is established by a cantilever test as outlined in AISI S907 (AISI, 2017a).

The method proposed by Seek and Murray utilizes displacement compatibility between the purlin and the panels to determine the forces interacting between a purlin and the panel. By equating the displacement of a Zee purlin that results from the applied load effects (unsymmetric bending and downslope forces) to the restoring displacements caused by the restraint provided by the panels, the forces interacting between the purlins and the panels can be determined. Accurately predicting the magnitude and the distribution of this forces is critical for determining the stabilizing forces on the purlin. It has an impact on the forces transferred to the anchorage devices, the torsion imparted on the purlin, the lateral displacement of the system and the corresponding second order effects that this deformation will cause.

Recent work by Plaut and Moen (2020) has shown that the flexibility of the connection between purlins and panels has an impact on the behavior of the system, particularly for standing seam systems. Additionally, Seek (2022) explored through finite element models how the behavior of the system changed with different levels of stiffness in the panels versus the clip connections. Therefore, it is desired to develop analytical models that include both shear flexibility in the panels as well as flexibility in the connections to better represent this behavior.

2. Diaphragm Models

Three different models of the distribution of the forces between the panels and purlins were investigated. The first model, utilizing pure shear behavior and developed by Seek and Murray, works well for through-fastened systems. With this model, the force distribution between the panels and the purlins is essentially uniform. As noted by Plaut and Moen (2020), for standing seam systems, the relative movement between the purlin and the panels that the clip allows can be modeled with a spring. This philosophy is explored with a model with linear springs between the purlin and the panels and a rigid diaphragm. With this philosophy, the forces take on a parabolic distribution. Finally, a model was developed that includes flexibility of the panels and includes a linear spring between the purlins and panels.

It should be noted that with these models of the purlin systems, although the purlins are subject to substantial torsion, it is assumed that additional restraints are provided, as in paired torsion braces as described by Seek and Avci (2023) that minimize the torsional rotation of the purlin along its span. In the absence of these torsional restraints, the torsional deformations affect the magnitude of the forces between the purlin and the panels. The restraining force provided by the panels will typically be reduced.

2.1 Diaphragm modeled with pure shear deformation

The displacement compatibility analysis methodology by Seek and Murray (2008) was developed based on through fastened panels assuming pure shear deformation in the panels. The displacement compatibility method quantifies the forces interacting between the purlins and

panels by considering the relative displacement between the purlins and the panels. A simply supported purlin loaded by a uniform load, w , in the plane of its web (no roof slope) without any lateral restraints will have the lateral deflection, Δ_{unrest} , at mid-span

$$\Delta_{\text{unrest}} = \frac{5w \left(\frac{I_{xy}}{I_x} \right) L^4}{384EI_{my}} \quad (1)$$

In Eq. (1), L is the span of the purlin, E is the modulus of elasticity of the purlin, I_x is the moment of inertia about the x-axis and I_{xy} is the product inertia relative to the orthogonal x- and y- axes perpendicular and parallel to the web respectively. The form of Eq (1) was introduced by Zetlin and Winter (1955) to allow the use of conventional deflection formulas to calculate deflections cross sections like Zees with inclined principal axes, rather than subdivide forces into components along the principal axes. The method utilizes the modified moment of inertia, I_{my} , and a fictitious lateral force, $w(I_{xy}/I_x)$. The modified moment of inertia about the y-axis is

$$I_{my} = \frac{I_x I_y - I_{xy}^2}{I_x} \quad (2)$$

It is important to note that the fictitious lateral force, $w(I_{xy}/I_x)$, is just a mathematical construct and there is no net horizontal force applied to the purlin.

When the restraint provided by the panels is considered, the force the purlin exerts on the diaphragm, w_{rest} is uniform along the length of the purlin. The resulting in-plane deflection of the diaphragm is

$$\Delta_{\text{diaph}} = \frac{w_{\text{rest}} L^2}{8G' b_{\text{diaph}}} \quad (3)$$

where, G' is the diaphragm stiffness and b_{diaph} is the width of the diaphragm tributary to the purlin. This displacement is the net diaphragm displacement of the system at mid-span. The net displacement of the purlin can also be considered as the unrestrained displacement minus the lateral displacement caused by the uniform force from the panels acting on the purlin.

$$\Delta_{\text{net}} = \frac{5w \left(\frac{I_{xy}}{I_x} \right) L^4}{384EI_{my}} - \frac{5w_{\text{rest}} L^4}{384EI_{my}} \quad (4)$$

By equating the displacement of the diaphragm with the net displacement of the purlin, the force, w_{rest} , interacting between the purlin and the panels can be quantified. That is,

$$w_{rest} = \frac{5w \left(\frac{I_{xy}}{I_x} \right) L^4}{384EI_{my} + \frac{5L^4}{384EI_{my}} + \frac{L^2}{8G'b_{diaph}}} \quad (5)$$

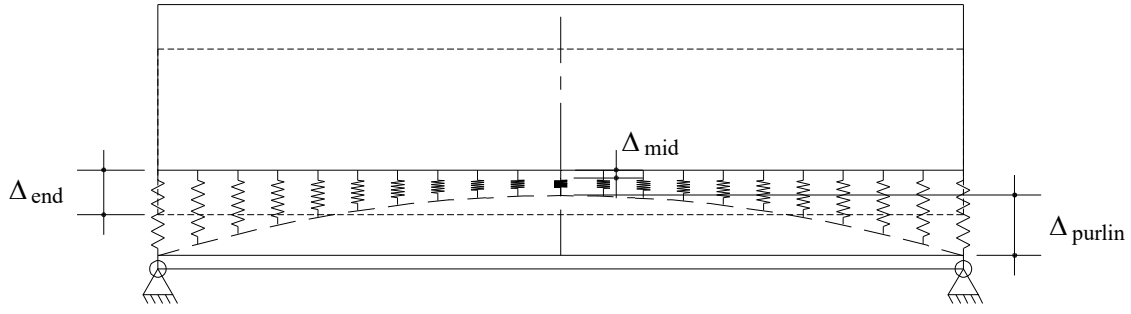
Once w_{rest} is determined, additional information such as the torsion effects on the purlin, biaxial bending forces and the distribution of forces through the diaphragm can be determined as shown by Seek and Murray (2008).

As previously noted, when the applied load, w , is perpendicular to the web of the purlin there should be no net horizontal force. Therefore, the uniform force along the length of the purlin must be balanced with an equal and opposite force at the ends of the purlin. For an ideal system with pure shear in the panels and rigid connections between the purlin and the panels, the force between the purlin and the panel at the ends of the purlin is $w_{rest}L/2$. This force can be substantial. Theoretically, this force is applied at the very end of the purlin (at the last connection between the purlin and the panel). For a through fastened system with rigid connections between the panels and the purlins, this model works well. However, when slip occurs in the connection between the purlin and panel, the distance over which this force is transferred increases and the peak force is reduced.

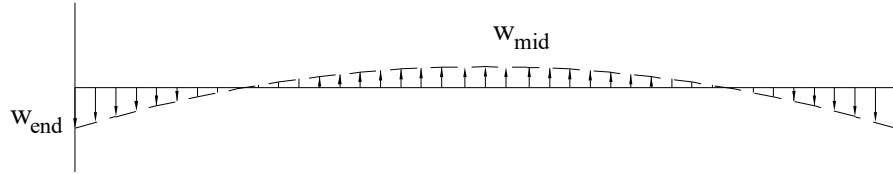
2.2 Diaphragm modeled with rigid panels and spring connections

To explore the influence of the flexibility of the connection between the purlin and the panels, the displacement compatibility method discussed in Section 2.1 is applied to a system with rigid panels and springs to represent the connection between the panels and the purlins. Plaut and Moen (2020) have developed a very powerful theoretical model with spring restraints, however, with this model, the springs are anchored externally. When considering the restraint provided by panels attached to the top flange, it is important to consider that the panel system is floating and connected by the springs. There will be some net lateral displacement of the rigid panel system, Δ_{end} , as shown in Fig. 1 a).

It is assumed that the lateral displacement of the purlin takes on a parabolic shape along its length with maximum displacements at the ends. Because the forces interacting between the purlin and the panel are a function of the deflection of the springs connecting them, the distribution of forces along the length of the purlin is taken as parabolic. The maximum force, w_{mid} , occurs at mid-span. As discussed in Section 2.1, when subjected to a force parallel to the web, there is no net horizontal force in the purlin. The positive forces acting along the length of the purlin must be counteracted by opposing forces at each end. The maximum counteracting force is w_{end} . The parabolic distribution of the forces is shown in Fig. 1 b).



a) System displacements



b) Distribution of lateral forces along span

Figure 1: Rigid panel with spring connections

Based on a parabolic shape for the load distribution, for the net sum of horizontal forces to be zero, the force at the end is twice the force at the midspan, that is $w_{end} = 2w_{mid}$. The equation for the parabolic distribution of forces along the length of the purlin is

$$w(x) = w_{mid} \left(-12 \left(\frac{x}{L} \right)^2 + 12 \left(\frac{x}{L} \right) - 2 \right) \quad (6)$$

Similar to Section 2.1, the forces acting between the purlin and the sheathing can be determined by displacement compatibility. For an applied uniform load, the maximum unrestrained displacement is as defined in Eq 1. The equation for the lateral deflection of the purlin at any point (x) along the length resulting from the parabolic restraining force from the panel is.

$$\Delta = \frac{w_{mid} L^4}{EI_{my}} \left(\frac{1}{30} \left(\frac{x}{L} \right)^6 - \frac{1}{10} \left(\frac{x}{L} \right)^5 + \frac{1}{12} \left(\frac{x}{L} \right)^4 - \frac{1}{60} \left(\frac{x}{L} \right) \right) \quad (7)$$

The maximum lateral deflection of the purlin at mid-span is

$$\Delta_{mid} = \frac{11}{1920} \frac{w_{mid} L^4}{EI} \quad (8)$$

The displacement of the panel system is derived entirely from the deformation of the springs between the purlin and the rigid panels. From equilibrium, the magnitude of the force at the end, w_{end} is twice that of the force at mid-span and of course acts in the opposite direction. Using a linear spring, since the displacement is directly proportional to the force, the displacement at the end, Δ_{end} , is twice the displacement at midspan. The net displacement of the panel system, Δ_{diaph}

= $3(w_{mid}/k_{clip})$ where k_{clip} is the stiffness of the clip connection per unit length. By equating the net displacement of the purlin with the displacement of the diaphragm, the force at mid-span can be determined.

$$w_{mid} = \frac{5}{384} \frac{w \left(\frac{I_{xy}}{I_x} \right) L^4}{\frac{11}{1920} \frac{L^4}{EI} + \frac{3}{k_{clip}}} \quad (9)$$

2.3 Diaphragm modeled with flexible panels and linear spring connections

In real purlin systems with standing seam diaphragms, the deformation of the system results from a combination of panel diaphragm flexibility and slip in the purlin-to-panel connections. The forces interacting between the purlin and the panels as modeled by shell finite element models (Seek, 2022) take on the general shape shown in Fig. 2 (Flexible panel-flexible clip) with an approximately uniform force along the middle of the span and gradual force reversal at the ends of the span. Of course, when the flexibility from the panels dominates, ie. stiff spring connections and flexible panels, the shape of the distribution of the forces will be closer to that shown in Fig. 2 for rigid clip – flexible panel, where the force is uniform along most of the span and there is a large force reversal at the ends. Conversely, when the flexibility of the clip connections dominates, ie stiff panel diaphragm and flexible spring connections, the shape of the distribution of forces will be closer to parabolic distribution discussed in section 2.2 and as shown in Fig. 2 for rigid panel – flexible clip.

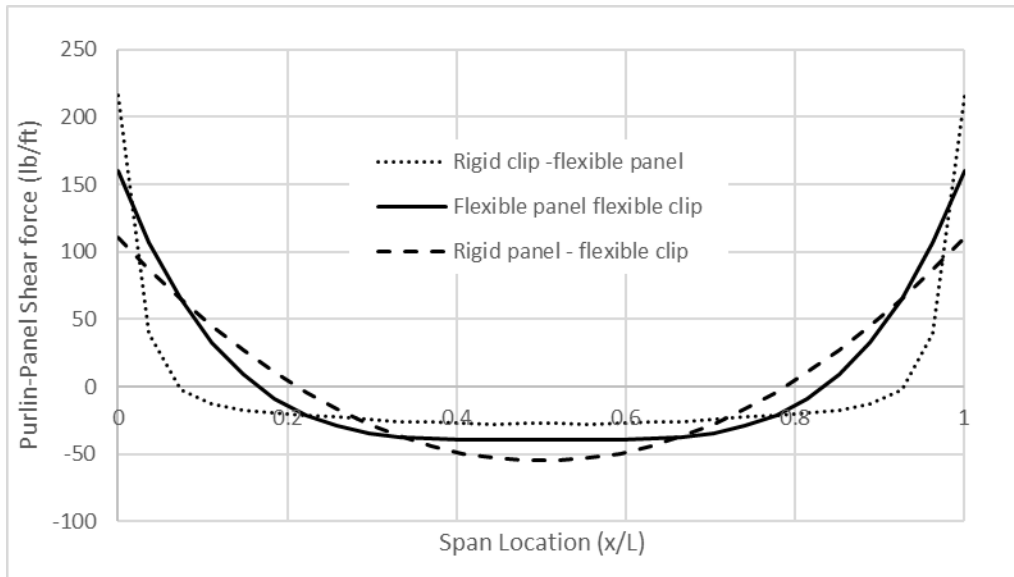


Figure 2: Purlin Panel shear forces for combinations of clip and panel flexibility

To model the case of typical systems to include flexibility panels and flexibility in the clip connections that can also capture the behavior at the ends of the spectrum, a 4th order

polynomial was chosen to represent the force interacting between the purlins and the panels along the length of the purlin. The general form of the polynomial is

$$w(x) = Ax^4 + Bx^3 + Cx^2 + Dx + E \quad (10)$$

The following boundary conditions were used to solve for the coefficients:

$$w(0) = w(L) = -w_{\text{end}}$$

$$w\left(\frac{L}{2}\right) = w_{\text{mid}}$$

$$w'\left(\frac{L}{2}\right) = 0$$

$$\int w(0) = \int w(L) = 0$$

$$\iint w(0) = \iint w(L) = 0$$

In the above boundary conditions, w_{end} is the magnitude of the distributed force at the end of the span and w_{mid} is the magnitude of the distributed force at the mid-span. For simplification, the relationship between w_{end} and w_{mid} is defined by the ratio α , where $\alpha = w_{\text{end}}/w_{\text{mid}}$.

The resulting equation for the distributed force along the length of the purlin is.

$$w(x) = w_{\text{mid}} \left[(80 - 40\alpha) \left(\frac{x}{L}\right)^4 + (-160 + 80\alpha) \left(\frac{x}{L}\right)^3 + (96 - 54\alpha) \left(\frac{x}{L}\right)^2 + (-16 + 14\alpha) \frac{x}{L} - \alpha \right] \quad (11)$$

The deformations of the system are shown in Fig. 3.

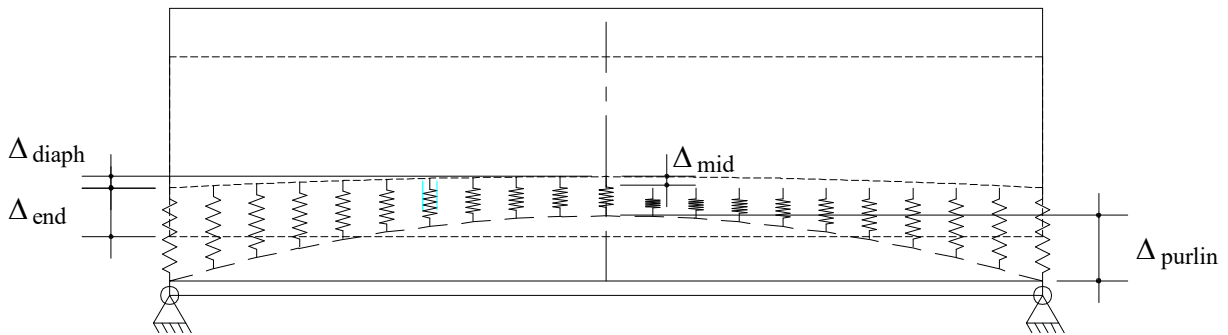


Figure 3: Deformation of system – flexible clips and flexible panels

The lateral deflection of the purlin due to the lateral restraining forces from the panels is

$$\Delta_p(x) = \frac{w_{mid}xL^3}{32EI_{my}} \left[\frac{16(2-\alpha)}{21} \left(\frac{x}{L}\right)^7 + \frac{64(-2+\alpha)}{21} \left(\frac{x}{L}\right)^6 + \frac{8(16-9\alpha)}{15} \left(\frac{x}{L}\right)^5 + \frac{8(-8+7\alpha)}{15} \left(\frac{x}{L}\right)^4 - \alpha \left(\frac{x}{L}\right)^3 + \frac{64-11\alpha}{210} \right] \quad (12)$$

Similarly, the shear deformation of the diaphragm that results from the distributed forces along the span is

$$\Delta_{diaph}(x) = \frac{w_{mid}x^2}{G'b_{diaph}} \left[\frac{4(2-\alpha)}{3} \left(\frac{x}{L}\right)^4 + 4(-2+\alpha) \left(\frac{x}{L}\right)^3 + \frac{(16-9\alpha)}{2} \left(\frac{x}{L}\right)^2 + \frac{(-8+7\alpha)}{3} \left(\frac{x}{L}\right) - \frac{\alpha}{2} \right] \quad (13)$$

To find the distribution of the forces between the purlin and the panels, because there are two degrees of freedom (diaphragm flexibility and spring deformation), two compatibility equations are required. Compatibility equations are developed at the third points of the purlin and at the midpoint of the purlin. By setting the compatibility equations at the third points and mid-points equal to each other, the magnitude of α is determined. Next, to determine the magnitude of w_{mid} , either the compatibility equation at the third points or mid-span can be used.

For compatibility at mid-span, the lateral deflection of the purlin resulting from the forces interacting between the purlin and the diaphragm is

$$\Delta_{p,mid} = \frac{w_{mid}L^4}{384EI_{my}} \left(\frac{186+61\alpha}{140} \right) \quad (14)$$

The in-plane deflection of the diaphragm at mid-span is

$$\Delta_{diaph} = \frac{w_{mid}L^2}{24G'b_{diaph}} \left[1 + \frac{\alpha}{4} \right] \quad (15)$$

To determine the magnitude of the force between the purlin and the panels, displacement compatibility is established at mid-span. That is, the unrestrained displacement at mid-span is equated to the net deformation of the system. The unrestrained displacement is from Eq. 1. There are four components of the deformation of the system (see Fig. 3): the deformation of the purlin due to the distributed load, the deformation of the diaphragm due to the distributed force, the clip spring displacement at mid-span and the clip displacement at the ends of the span. The compatibility equation is

$$\frac{5w \left(\frac{I_{xy}}{I_x} \right) L^4}{384EI_{my}} = w_{mid} \left[\frac{L^4}{384EI_{my}} \left(\frac{186+61\alpha}{140} \right) + \frac{L^2}{24G'b_{diaph}} \left[1 + \frac{\alpha}{4} \right] + \frac{1+\alpha}{k_{clip}} \right] \quad (16)$$

For compatibility at the purlin third points, the unrestrained lateral deflection of the purlin resulting from the applied uniform gravity load is

$$\Delta_{\text{unrest}} = \frac{11wL^4}{972EI_{\text{my}}} \quad (17)$$

The lateral displacement of the purlin at third points due to the distributed force between the purlin and the panel is

$$\Delta_{\text{p,3rd}} = \frac{w_{\text{mid}}L^4}{12EI_{\text{my}}} \left(\frac{8024 + 2729\alpha}{229635} \right) \quad (18)$$

At the third point, the deflection of the diaphragm due to the in-plane forces is

$$\Delta_{\text{diaph,3rd}} = \frac{w_{\text{mid}}L^2}{9G'b_{\text{diaph}}} \left[\frac{64 + 22\alpha}{243} \right] \quad (19)$$

The displacement of the spring connection at the third point is determined from force between the purlin and panel from Eq 11 at $x = L/3$, that is

$$w\left(\frac{L}{3}\right) = w_{\text{mid}} \left[\frac{32 + 11\alpha}{81} \right] \quad (20)$$

The compatibility equation therefore at the third point of the purlin is calculated such that the unrestrained displacement equals the sum of the restraining displacements of the system.

$$\frac{11wL^4}{972EI_{\text{my}}} = \frac{w_{\text{mid}}L^4}{12EI_{\text{my}}} \left(\frac{8024 + 2729\alpha}{229635} \right) + \frac{w_{\text{mid}}L^2}{9G'b_{\text{diaph}}} \left[\frac{64 + 22\alpha}{243} \right] + \frac{w_{\text{mid}}}{k_{\text{clip}}} \left[\frac{32 + 11\alpha}{81} \right] + \frac{w_{\text{mid}}\alpha}{k_{\text{clip}}} \quad (21)$$

In Eqs. 16 and 21, the only unknowns are w_{mid} and α . Both equations can be easily rearranged to solve for w_{mid} .

$$w_{\text{mid}} = \frac{5w \left(\frac{I_{\text{xy}}}{I_x} \right) L^4}{384EI_{\text{my}}} \quad (16a)$$

$$= \frac{L^4}{384EI_{\text{my}}} \left(\frac{186 + 61\alpha}{140} \right) + \frac{L^2}{24G'b_{\text{diaph}}} \left[1 + \frac{\alpha}{4} \right] + \frac{1 + \alpha}{k_{\text{clip}}}$$

$$w_{\text{mid}} = \frac{11w \left(\frac{I_{xy}}{I_x} \right) L^4}{972EI_{my}} \quad (21a)$$

$$= \frac{L^4}{12EI_{my}} \left(\frac{8024 + 2729\alpha}{229635} \right) + \frac{L^2}{9G'b_{\text{diaph}}} \left[\frac{64 + 22\alpha}{243} \right] + \frac{32 + 92\alpha}{k_{\text{clip}}}$$

By setting these two equations equal to each other and using an iterative equation solver such as *Goal Seek* in Excel, the value of α may be determined. The value of α will vary depending on the relative stiffness between the spring and the diaphragm. As the stiffness of the diaphragm increases relative to the stiffness of the springs, the value of α will approach a value of 2 which is the theoretical value for a parabolic load distribution resulting from a rigid diaphragm/spring relationship discussed in Section 2.2.

Once the value of α is determined, either Eq. 16a or 21a can be solved for w_{mid} . To determine the distribution of the forces along the span, Eq. 11 can be used.

3. Comparison of Equations to Finite Element models

The method presented in section 2.3 is compared to finite element models presented by Seek (2022). The models used by Seek are based on the base test results presented by Emde (2010). Emde performed tests on a series of purlins from a single manufacturer. The analysis presented here is based on two series of tests performed on 8 in. deep Zees (8ZSx2.75x057) and (8ZSx2.75x100). Specifically, the results are used from test ID 8Z16A and 8Z12D. The properties of each of these purlins is provided in Table 1.

Table 1: Purlin Properties

Property	8ZS2.75x057	8ZS2.75x100
Depth, d (in.)	8.00	8.00
Flange width, b (in.)	2.75	2.75
Thickness, t (in.)	0.057	0.100
I_x , (in. ⁴)	8.158	14.191
I_y , (in. ⁴)	1.158	2.275
I_{xy} , (in. ⁴)	2.229	4.145
I_{my} , (in. ⁴)	0.549	1.064
I_{mx} , (in. ⁴)	3.867	6.639

The tests were performed in a vacuum chamber 8 feet wide. The purlins were spaced at 5 feet on center and spanned 27 feet. Standing seam panels 7 feet wide were placed on top of the purlins leaving a 6 in. gap on either side of the chamber. The resulting tributary width on each purlin is 3.75 ft. The standing seam panels were attached to the purlins with a low sliding clip with a ½” thermal block below the clip.

To model these purlins, Seek (2022) created a shell finite element model in SAP 2000. With this shell finite element model, the web of the purlin was discretized into 4 elements, each flange was discretized into 3 elements and a single element was used for the flange stiffener. Sharp corners were used at the intersections between the web, flange, and stiffeners. Along the length of the

purlin, the length of the elements was 2 in. To model the diaphragm, the standing seam panels were discretized into 12 in. square elements. The panels were assigned a membrane thickness equivalent to the thickness of the panels (0.0197 in.). The diaphragm shear stiffness, G' , was adjusted by changing the shear modulus, G , of the panel material. For a desired diaphragm stiffness in the panel, the required shear modulus in the model was calculated by $G = G'/t$ where t is the thickness of the panel.

The clips connecting the purlin to the panel were modeled as 2-node link spring elements. With these link elements, the spring stiffness of this connection could be directly defined. Seek (2022) created models with both linear springs and non-linear springs to investigate how introducing flexibility in the connection between the purlin and the panel affected the behavior. The analytical method presented in Section 2.3 is compared to the results of the models using linear springs.

Three models were created for each purlin cross section. The first model utilized a rigid connection between the purlin and the panels and all of the diaphragm flexibility was derived from pure shear deformation of the panels. Seek (2018) observed that the shear deformation behavior of the diaphragm was highly nonlinear. Therefore, the shear stiffness of the panel, G' , was chosen to align with this original analytical work by Seek, who chose stiffness panel shear stiffness values that predicted lateral deflections that matched the lateral deflection reported in the tests by Emde. Two additional models were created with springs with a finite stiffness. The springs were arbitrarily chosen with spring stiffness of 100 lb/in/ft and 50 lb/in/ft. The panel shear stiffness, G' , for each model was adjusted such that the lateral deflection of the test matched the lateral deflection of the model with rigid connections between the purlin and the panel. For comparing the analytical model developed in Section 2.3 to the finite element models, the same panel shear stiffness reported by Seek (2022) was used in the analytical models. A summary of the tests, the diaphragm shear stiffness, and the lateral deflection from the tests, FE model and analytical model are shown in Table 2. Note that in Table 2, the lateral deflection of the test, finite element model, and analytical model are provided.

Table 2: Model Summary

Purlin	Designation	Link stiffness (lb/in)	Max Pressure (psf)	Uniform load, w (lb/ft)	Diaphragm stiffness, G' (lb/in)	Δ_{mid} Tested (in.)	Δ_{mid} FE Model (in.)	Δ_{mid} Analytical (in.)
8Zx057	1A-Tested		17.68			1.86		
	U2-rigid	Rigid		66.3	230		2.13	1.82
	U2-100	100		66.3	460		2.14	2.16
	U2-50	50		66.3	3000		2.18	2.35
8Zx100	2D - Tested		37.65			6.17		
	U2-rigid	Rigid		141.2	110		5.89	6.17
	U2-100	100		141.2	155		5.91	6.43
	U2-50	50		141.2	230		5.91	6.60

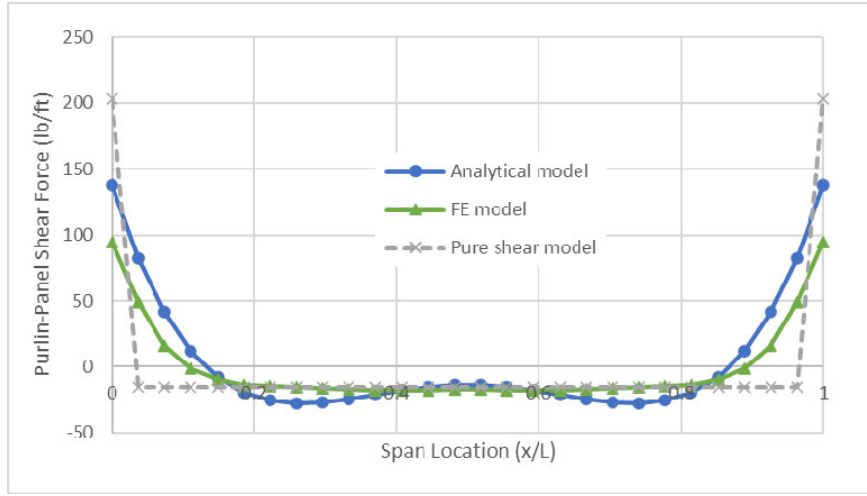
A summary of the comparison between the forces between the panel and the purlin is shown in Table 3. Plots of each of the models is shown in Figures 4 and 5. In Table 3, the value of α is shown for both the FE model results and that predicted by the analytical model. As the spring stiffness decreases, the value of α predicted by the analytical method more closely matches that of the FE model. It should be noted that when predicting α by the analytical model, it is

sensitive and could show some variation depending on the precision used in the solution method to solve for α . Table 3 also shows the magnitude of the forces interacting between purlin and panel at the key points (mid-span and ends). Based on these values, the correlation does not appear to be very good, however the plotted results in Figures 4 and 5 are more telling where the shape of the analytical curve follows the trends in the FE model. When the flexibility of the diaphragm is derived primarily from pure shear in the panels, the forces between the purlin and the panel are fairly uniform along the span and there is a sharp transition at the ends. As the flexibility of the diaphragm transitions from being derived primarily from panel shear to having a contribution from flexibility in the connection between the purlin and the panel, the transition softens at the ends and has a slight curvature along the middle. This follows the theory to the other end of the spectrum, where if all of the flexibility of the system is derived from flexibility in the spring connections, the shape of the distribution of forces will be parabolic and match the values from Eq 6. In general, the analytical model predicts slightly higher forces than the FE models at both mid-span and at the ends of the purlin. Additionally, as the flexibility is more dominated by the spring stiffness, the total deflection predicted by the analytical model increases relative to that predicted by the FE models for the same input values of spring stiffness and panel diaphragm stiffness.

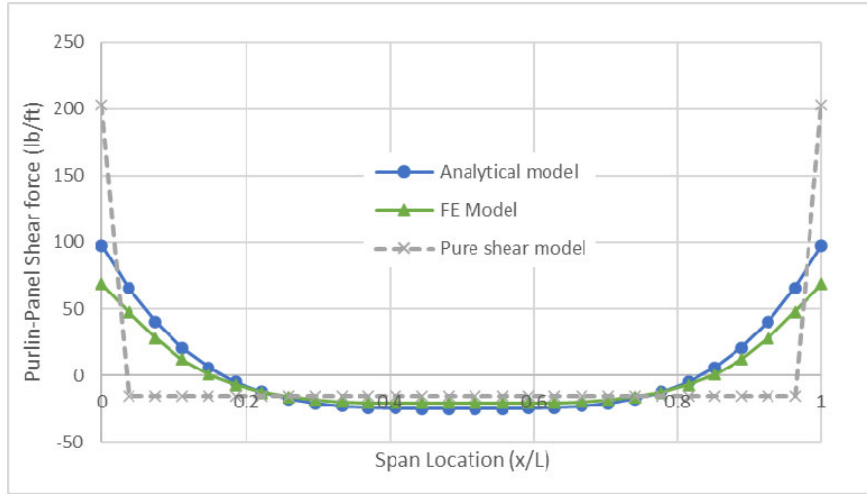
One key advantage of the new method is that it much more closely aligns with the maximum force at the end of the panel. The analytical method from Section 2.1 predicts much larger forces at the ends of the purlin. These forces are compounded at anchorage locations for systems with multiple purlin lines. The modified method of Section 2.3 shows, like finite element models, that the reversal of forces is more gradual and the peak force at the ends is greatly reduced (typically by about half or more). With the more gradual reversal of forces, the torsional effects on the purlins resulting from the lateral restraint by the panels are also reduced which can reduce the predicted torsional stresses, bracing and anchorage forces.

Table 3: Comparison FE Model to Analytical Model

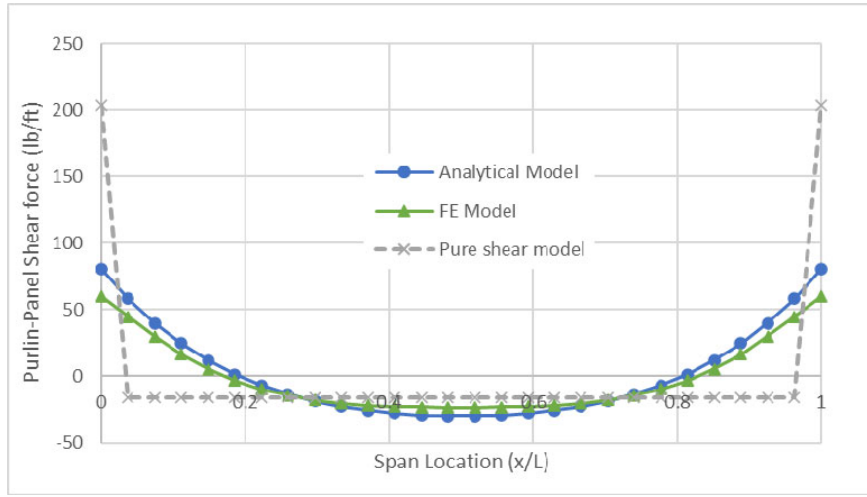
Purlin	Designation	α		W_{mid} (lb/ft)		W_{end} (lb/ft)	
		FE Model	Analytical	FE Model	Analytical	FE Model	Analytical
8Zx057	U2-rigid	5.525	10.000	17.11	13.77	94.54	137.7
	U2-100	3.326	3.904	20.58	25.06	68.425	97.8
	U2-50	2.549	2.685	23.46	29.89	59.775	80.2
8Zx100	U2-rigid	7.909	7.641	27.37	26.87	216.42	205.3
	U2-100	3.834	4.070	32.82	39.27	125.845	159.8
	U2-50	2.812	2.911	37.60	46.03	105.715	134.0



c) Results for rigid link

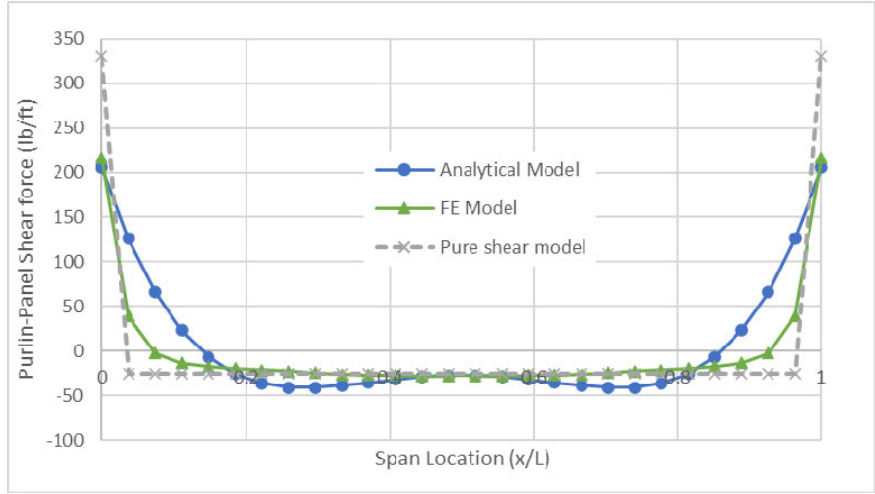


b) Results for link $k=100\text{lb/in/ft}$

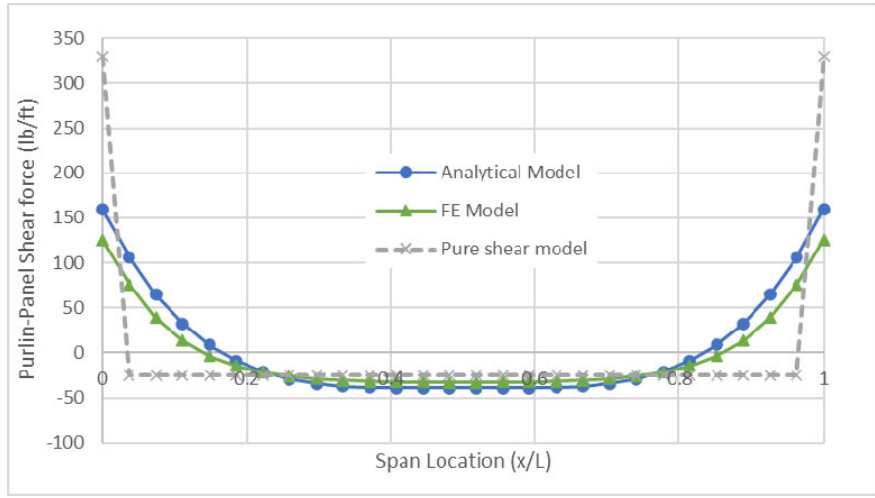


a) Results for link $k=50\text{lb/in/ft}$

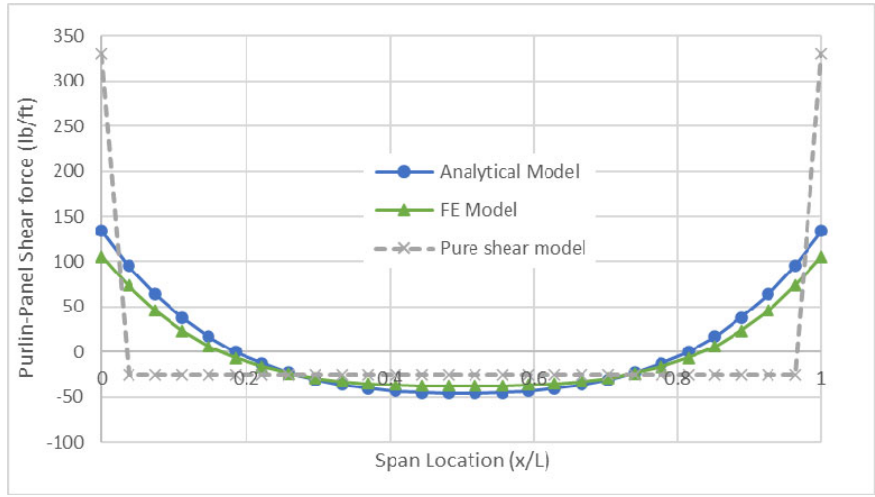
Figure 4: Panel Shear Force for 8ZS2.75x057



c) Results for rigid link



b) Results for link $k=100$ lb/in/ft



a) Results for link $k=50$ lb/in/ft

Figure 5: Panel Shear Force for 8ZS2.75x100

4. Conclusions

Analytical methods to predict the forces interacting between Z-section purlins and the panel system providing lateral restraint have been presented. The first method presented in Section 2.1 is a previously developed model where all of the flexibility of the panel system is derived from panel shear flexibility. The second method presented in Section 2.2 provides bounds at the other end of the spectrum where the panels are considered rigid and the connections between the purlins and panels are considered flexible. The final method presented in Section 2.3 analyzes the interaction between the purlin and the panel with flexibility derived both from panel shear flexibility and flexibility in the connection between the purlin and the panel system. The analytical method developed in Section 2.3 is compared to shell finite element models of purlins systems that are modeled with both shear flexibility in the panels and flexibility in the connections between the purlins and the panels. Correlation of the proposed method with finite element models is not perfect, but the method shows much better correlation than methods that ignore the flexibility of the purlin-panel connection and in general follows the trends in behavior as the dominant flexibility shifts from the panels to the connections. Because the force interacting between the purlin and the panels is integral to the overall behavior and performance of purlins, by better predicting the distribution of the forces interacting between the panel and purlin, more accurate predictions of torsion and lateral flexural effects can be developed.

References

- AISI (American Iron and Steel Institute) (2016) *SI100-16 North American Specification for the Design of Cold-Formed Steel Structural Members*. AISI. Washington, DC. 2016.
- AISI (American Iron and Steel Institute) (2017a) S907-17 Test Standard for Determining the Strength and Stiffness of Cold-Formed Steel Diaphragms using the Cantilever Test Method. AISI. Washington, DC. 2017.
- AISI (American Iron and Steel Institute) (2017b). S908-17 Base Test Method for Purlins Supporting a Standing Seam Roof System. AISI. Washington, DC. 2017.
- Emde, M. G. (2010) Investigation of Torsional Bracing of Cold-Formed Steel Roofing Systems. Master's Thesis. University of Oklahoma. Norman, OK. 2010.
- Plaut, R.H. and Moen, C. D. (2020). "Lateral-Torsional Deformations of C- and Z-section beams with continuous bracing." *Proceedings of the Annual Stability Conference Structural Stability Research Council*. SSRC, Chicago, IL.
- Seek, M. W., Murray, T.M. (2008) "Lateral restraint forces in Z-section roof systems using the component stiffness method." *Journal of Constructional Steel Research*, 64 (12), December 2008. 1366-1378.
- Seek, M. W. (2018). "Flexural Strength of continuous-span Z-purlins with paired torsion braces using the Direct Strength Method". *Proceedings of the 24th International Specialty Conference on Cold-Formed Steel Structures*. 2018.
- Seek, M. W. (2022) "Exploring the effects of clip flexibility on the behavior of standing seam diaphragms to brace cold formed steel purlins." *Conference Proceedings, Structural Stability Research Council Annual Stability Conference*. 2022. Structural Stability Research Council, Chicago, IL.
- Seek, M. W., Avci, O. (2023) Evaluation of local and distortional buckling strength of purlins with paired torsion bracing using Direct Strength Method, *Journal of Constructional Steel Research*, V 203, 2023,
- Zetlin, L and G. Winter. (1955). "Unsymmetrical Bending of Beams with and without Lateral Bracing." *Journal of the Structural Division*, ASCE, Vol. 81, 1955.